OPTIMAL SIZE AND POSITION OF THE PLANAR BACK REFLECTOR MOVEABLE ONLY IN THE DIRECTION NORMAL TO THE BIFACIAL SOLAR COLLECTOR PLANE

Novak N. NIKOLIĆ[1*], Nebojša S. LUKIĆ[1], Aleksandar M. NEŠOVIĆ[1], Danijela M. NIKOLIĆ[1]

[1] University of Kragujevac, Faculty of Engineering, Sestre Janjić 6, 34000 Kragujevac, Serbia

Corresponding author; E-mail: novak.nikolic@kg.ac.rs

Abstract: *In this paper, the concept of a collector-reflector system consisting of a bifacial solar collector and a single flat-plate reflector separated and placed in parallel below the collector but moveable only in the direction normal to the collector plane is investigated. The developed mathematical model was used to optimize the size and position of the planar back reflector. The optimal hourly, daily, monthly and annual distances between the collector and reflector were determined. In addition, the daily, monthly and annual energy performance of the optimized bifacial collector-reflector system was estimated and compared with that of the corresponding monofacial solar collector. Based on the obtained results, two ways of use of the reflector are recommended, either according to the optimal hourly (moveable reflector) or optimal annual (fixed reflector) reflector positions. With optimally positioned moveable or fixed reflector the total solar radiation incident on the bifacial solar collector can be significantly higher than that for a monofacial solar collector. Its largest daily and monthly as well as average annual increase is: 74% (59%), 65.91% (46.21%) and 54% (39.4%), respectively. The proposed model can be applied to evaluate the energy performance of flat-plate bifacial thermal, photovoltaic or photovoltaic-thermal solar collector, of arbitrary size and position, which is in this arrangement with a planar reflector.*

Key words*: solar collector, bifacial, reflector, optimal position, optimal size, mathematical model*

1. Introduction

Solar energy is a renewable resource that has the potential to provide a lifetime supply of energy. There are various methods available for harnessing solar energy, and they differ in how they capture, convert, and distribute sunlight to generate useful outputs [1]. A flat-plate solar collector is one of the simplest and most common device that captures incoming solar radiation. Many investigations have been conducted to improve the overall performance of a flat-plate thermal (FPC), photovoltaic (PV) and photovoltaic thermal (PVT) solar collectors. One of the simplest and most inexpensive solution is the utilization of one or more flat-plate reflectors coupled with either monofacial solar collector (MSC) or bifacial solar collector (BSC) in different configurations. There are studies of MSC integrated with a single top reflector [2], single bottom reflector [3], side (left and right) reflectors [4,5], top and bottom reflectors [6] and four reflectors (top, bottom, left and right) [7,8]. The numerical and experimental results exhibited that the MSC performance can be increased

by: 19.8% (FPC) [2]; 34.16% (PV) [3]; 26.1% (FPC) [4]; 35% (PV) [5]; 14.7% (PVT) [6]; 50% (FPC) [7] and 64% (FPC) [8]. As expected, the MSC with multiple reflectors has the highest energy yield, but is more complex, expensive and bulky.

FPC, PV or PVT system can be more cost-effective and energy efficient with the implementation of a bifacial solar absorber and plane reflector. This concept was first reported by Souka and Safwat [9,10]. A bifacial FPC (BFPC) tilted at 40˚ with five aluminium reflectors set behind it at angle of 60˚ was theoretically and experimentally evaluated. The maximum obtained thermal power of this BFPC was 48% higher than that for a FPC. However, these authors did not discuss the optimal reflector dimensions and the optimal distances between the reflector and the collector. Durković and Đurišić [11] stated that an optimally tilted bifacial PV (BPV) power plant would have 29.19% higher electricity production than a vertical BPV power plant if the distance between PV rows is 4 m and the coefficient of reflection (horizontal reflector) is 0.2. Zahid et al. [12] experimentally confirmed that the optimally tilted moveable front and rear mirrors can enhance the power generation of the vertical BPV by up to 57% during autumn equinox and 51% for the entire year. The main drawback of the proposed system is that it requires a relatively large horizontal surface for its installation. Khan et al. [13] predict that for almost all regions of the world vertical BPV farms will outperform monofacial PV farms by 10-20%, assuming a constant ground albedo equal to 0.5. In [14] and [15] a tilted BPV mounted on the ground covered with aluminum reflective surface was explored. The experimentally obtained average bifacial gain of the BPV was 16.54% and 21.4%, respectively. Optimization of the reflector size and its distace from the collector was not considered. Chen et al. [16] examined the effect of distance between wall and a tilted BPV module on electrical performance of a vertical BPV module. According to the tests conducted, unfortunately, only during one day, the highest bifacial gain can be reached when their distance is 1-1.5 times the size (width) of the BPV module. A tilted BPV modules combined with horizontal single-axis tracking reflector system were theoretically and experimentally considered in [17]. The results demonstrate that the average annual bifacial gain with tracking and fixed reflector is 30% and 17%, respectively. The performance of this system is limited since the back reflector is smaller than the module.

With a parallel arrangement of a BSC and a flat-plate reflector a higher performance of the BSC can be achieved, but if certain conditions are met: the size and distance of the reflector from the absorber are appropriate and the reflection is specular. In other words, the greatest advantage of the parallelism between the BSC and reflector is that the incident angle of the solar beam falling on the upper absorber surface can be the same as the incident angle of the solar beam falling on the lower absorber surface (BLAS). Anyway, this concept was investigated in [18-25]. The reflector can be either integrated with the BSC within the same housing [18-21] or be separated from the BSC housing [22-25]. Ooshaksaraei et al. [18] experimentally evaluated the power output of a BPV module, composed of four silicon solar cells (packing factor 0.69), coupled with a semimirror back reflector. An increase in power output of 20% was achieved for the distance between the BPV panel and the reflector of 115 mm. Lo et al. [19] optimized the design of the BPV panel, consisting of six solar cells (packing factor 0.33), with a back mirror reflector. They demonstrated that the maximum yearly electrical energy enhancement of the BPV of 26% can be obtained when the distance between the BPV and the mirror is 158 mm. The energy behaviour of a double-pass bifacial PVT (BPVT) solar air collector integrated with a v-groove back mirror was simulated in [20]. Total energy efficiency of the BPVT (packing factor=0.66, distance=100 mm) was found to be 9% higher than that for a monofacial

PVT under the same operating conditions. In [21] the double-path parallel flow BPVT (packing factor 0.67), equipped with a flat back aluminum reflector with 50 mm separation, was experimentally investigated. The total energy efficiency of 51%-67% was observed.

The biggest limitation of using a BSC integrated with a reflector within the same housing is that during most of the day and year, it is not possible to achieve full irradiation of the BLAS due to the shadow effect. The shadow on the reflector is caused by the lateral housing surfaces, BSC which is at a relatively small distance from the reflector and its packing factor. The aforementioned limitation is removed by moving the reflector away from the BSC, which requires the solar collector to be separated from the reflector structure. Robles-Ocampo et al. [22] designed and constructed a system consisting of a water-based BPVT and a set of stainless steel reflectors. The dimensions of the reflectors and its separation from the BPVT were not optimized. In comparison to the conventional PVT the proposed BPVT produced 40% larger amount of electricity. The collector-reflector system (CRS) with a flat-plate reflector placed in parallel below the BSC and movable in all three possible orthogonal directions: north-south, east-west and normal to the collector, was experimentally evaluated in [23]. The reflector dimensions were the same as those of the BSC. According to the experimental measurements thermal output of this BFPC was significantly higher (41.79-66.44%) than thermal output of the FPC. A bifacial and monofacial double-flow solar air heaters with a corrugated and flat-plate absorber were analytically studied in [24]. Under the assumption that the planar back reflector always enables full irradiation of the BLAS the maximum increase in thermal efficiency of 10.85% for the BFPC with a corrugated absorber over the FPC with a flat-plate absorber can be reached. Mandal and Ghosh [25] estimated the operation of a single-pass FPC and a double-pass BFPC with planar mirror reflector placed in parallel behind it. Both the BFPC and the reflector were moved with the position of the sun. Their dimensions were the same. The experimental results revealed that the double-pass BFPC has the higher efficiency (47.98%) than the single-pass FPC (38.1%). However, the compared results were not taken at the same time of the year. In [24,25] the authors did not optimize the distance between the collector and the reflector.

In this paper, the concept of a CRS consisting of a BSC and a single flat-plate reflector separated and placed in parallel below the collector but moveable only in the direction normal to the collector plane is presented and investigated. The novelty and contribution of the present research work rely on optimization of the size and position of the reflector. For the first time, the optimal size of the reflector and the optimal hourly, daily, monthly and annual distances between the collector and reflector were determined. In addition, the daily, monthly and annual energy performance of the optimized proposed bifacial CRS was estimated and compared with that of the corresponding MSC.

2. Methodology

2.1. Mathematical model

2.1.1 Total solar radiation incident on the collector surface

The amount of total solar radiation incident on the MSC (H'_{cG} [W/m^2]) and BSC (H'_{dG} [W/m^2]) surface is calculated according to eqs. 1 and 2, respectively [23]:

$$H'_{cG} = H'_{dir} \cdot \frac{\cos(i)}{\sin(\beta)} + H'_{dif} \frac{1+\cos(G)}{2} \quad (1)$$

$$H'_{dG} = H'_{dir} \cdot \frac{\cos(i)}{\sin(\beta)} + H'_{dif} \frac{1+\cos(G)}{2} + \rho \cdot H'_{dir} \cdot \frac{\cos(i_r)}{\sin(\beta)} \cdot \frac{A_{irr}}{A_{clow}} + \rho \cdot H'_{dif} \cdot \frac{A_r \cdot F_{rc}}{A_{clow}} \quad (2)$$

where H'_{dir} and H'_{dif} [W/m^2] are the intensities of the direct and diffuse solar radiation on a horizontal surface; i [rad] is the incident angle of the solar beam; β [rad] is the solar altitude angle; G [rad] is the collector tilt angle; ρ [-] is the coefficient of reflection for the reflector; i_r [rad] is the incident angle of the reflected beam; A_{irr} [m^2] is the size of the irradiated area on the BLAS; $A_{clow}=A_{cup}=A_c$ [m^2] is the area of the lower (upper) BSC surface; A_r [m^2] is the area of the reflector surface and F_{rc} [-] is the view factor. It should be noted that the diffuse radiation, reflected from the surrounding surfaces and reflector onto the both collectors, is neglected in the calculations.

2.1.2 Irradiated area A_{irr}

In order to achieve the highest possible performance of the BSC its lower surface should be fully irradiated at all times. In other words, for an arbitrary sun and reflector position the ratio A_{irr}/A_{clow} should be equal to 1 (eq. 2). According to the findings in [23], there are two ways to develop and optimize the bifacial CRS. The first way implies that the reflector has the same dimensions as the collector ($L_r=L_c$ and $W_r=W_c$) and be moveable in all three possible directions: north-south, east-west and normal to the collector and reflector plane. The second type of CRS consists of a BSC with a reflector that would move only in one direction, in the direction normal to the CRS plane. The greatest advantage of this system is reflected in the fact that the reflector moves significantly less, which makes it easier to build a structure for its movement. In order to achieve the highest possible irradiance of the BLAS, the dimensions of the reflector must be larger than the dimensions of the BSC ($L_r>L_c$ and $W_r>W_c$). To determine both the optimal size and the optimal hourly, daily, monthly and annual positions of the reflector of this type of CRS, the equations given in the Appendix A, derived according to the verified procedure explained in [26], would be used.

The CRS is observed in three planes: the plane perpendicular to the CRS plane with a view from the south (the EWGα plane), the plane perpendicular to the CRS plane with a view from the west (the NSGα plane) and the CRS plane (fig. 1). The parameters λ, ξ and a_p represent the length of irradiation in the EWGα, NSGα and CRS planes, whereas the parameter $b_{pnsG\alpha}$ represents the shadow length in the NSGα plane, respectively. The length parameters $p_{ewG\alpha}$ and $p_{nsG\alpha}$ are defined as the distance between the place where the sun beam hits the reflector and the place where the reflected beam hits the BLAS in the EWGα and the NSGα planes, respectively. The distance between the collector and the reflector plane is defined by y. The parameters $\beta_{ewG\alpha}$ and $\beta_{nsG\alpha}$ are projections of the solar altitude angle on the EWGα and the NSGα planes, whereas the parameter $\gamma_{G\alpha}$ is the projection of the solar azimuth angle on the CRS plane.

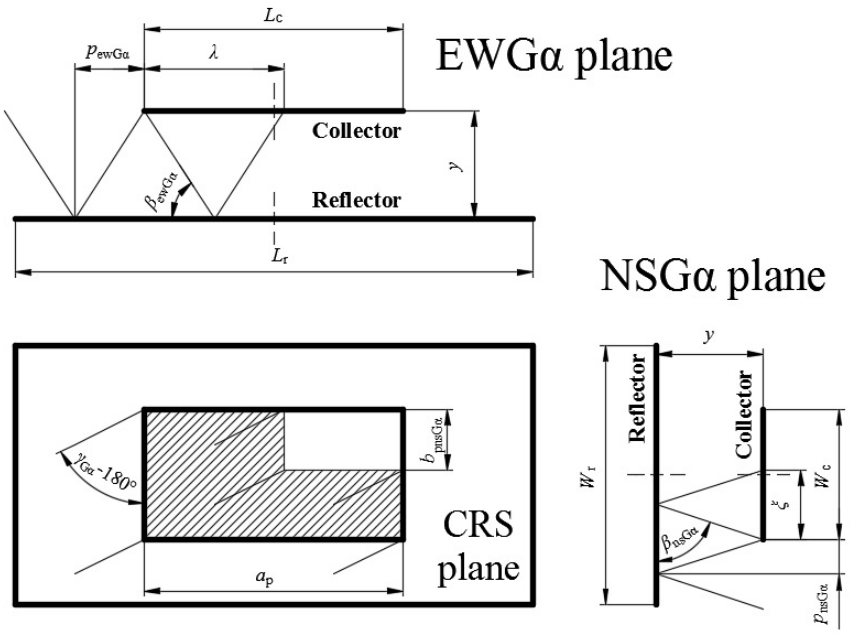

Figure 1. The proposed collector-reflector system observed in all three orthogonal planes: EWGα, NSGα and CRS plane

2.2. Simulation case

The dimensions of the BSC, L_c=1 m and W_c=0.5 m were chosen. The position of the considered CRS, its tilt angle of G=37.5˚ and orientation of α=180˚, corresponds to the annual optimal position of the solar collector for the city of Kragujevac (latitude 44.02 N, longitude 20.92 E) [27]. For practical reasons, the movement of the reflector is limited to a value of y=1 m, which corresponds to the collector length of L_c=1 m ($0 \leq y \leq L_c$). The step of changing y is 0.005 m. The optimal size and paths of the reflector were obtained numerically using FORTRAN. To simulate weather conditions of the selected location the EnergyPlus weather file (EPW file) was used. This file contains real weather data representing the long-term typical weather condition over a year in the city of Kragujevac [28]. For the purposes of calculating the incident solar radiation by using the eqs. 1 and 2, the hourly values of the H'_{dir} and H'_{dif} (8 a.m.-4 p.m.) were taken from the mentioned EPW file. It was assumed that ρ=0.9.

3. Results and discussion

Determining the optimal positions of the reflector (fig. 2) was preceded by the calculation of its optimal surface. As an initial value, it was adopted that the reflector surface is proportionally 10% larger than the collector surface, that is, L_r=1.1 m and W_r=0.55 m. For these reflector dimensions, the variable A_{irr} was calculated. In each subsequent step, the reflector surface was increased by 5% with recalculation of A_{irr}. This procedure was repeated until the moment when the average percentage annual deviation of A_{irr} for two adjacent steps (two close reflector dimensions) was very small (<0.3%). In this way, the optimal reflector dimensions of L_r=2 m and W_r=1 m were obtained.

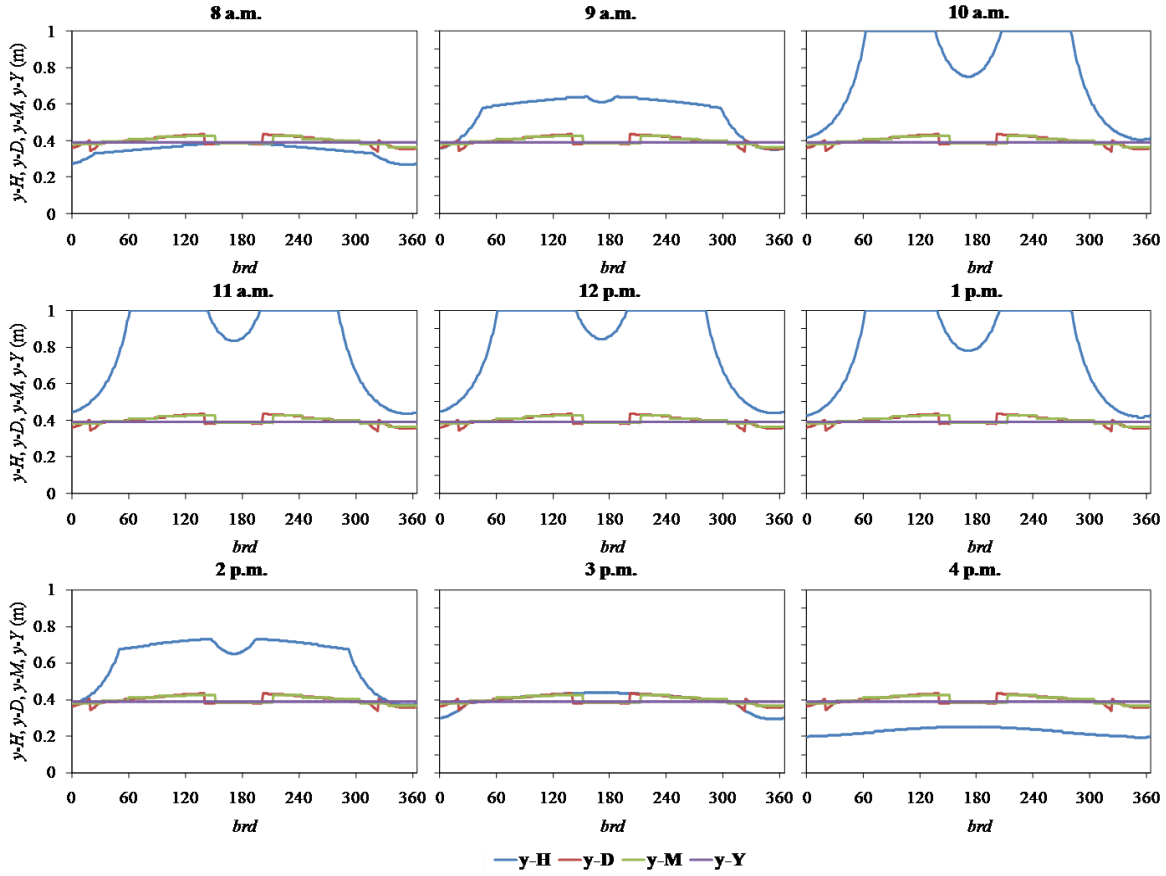

Figure 2. Optimal hourly (*y-H*), daily (*y-D*), monthly (*y-M*) and annual (*y-Y*) reflector positions

It is clear that the optimal reflector surface must be four times larger than the collector surface (A_r/A_c=4). In previously described bifacial CRS concepts, the reflector size was not optimized. Moreover, the A_r/A_c ratio had a significantly higher value. For instance, in [9,10] the authors used a reflector that was 7.6 times larger than the collector, while in [22] its size was 6.7 times larger. Optimal hourly reflector position represents the smallest possible distance of the reflector from the collector, at that hour, for which A_{irr} has the highest possible value. The distance *y-D* is that *y* for which the average daily A_{irr} has the highest value. The same pattern is applied to find *y-M* and *y-Y*. In fig. 3 the values of A_{irr}, for every hour (8 a.m.-4 p.m.) and every day of the year, calculated according to the adopted values for *y-H*, *y-D*, *y-M* and *y-Y*, are shown.

By observing fig. 2 and 3 at the annual and daily level, all diagrams for *y* and A_{irr} are symmetrical with respect to the summer solstice (22nd of June) and noon, respectively. The smallest *y-H* is in the morning and afternoon hours, at low values of the solar altitude angle (fig. 2). As its value increases, it is necessary to move the reflector away from the solar collector until noon, and then move it closer to the collector at sunset. On an annual basis, around noon, *y-H* increases from the beginning of the year until the period around the spring equinox, when it has its highest value, and then decreases until the summer solstice. From the summer solstice it increases again until the autumn equinox, when it has its highest value again, and after which it decreases until the end of the year. The parallelism of the reflector and collector and the optimal annual position of the CRS influenced the fact that the greatest distance of the reflector ($y=L_c$=1 m), is in the period of the year around spring (autumn) equinox and around noon (10 a.m.-1 p.m.) during the day ($i=i_r\approx0$). This results in a decrease in A_{irr}-*H*

(fig. 3) which is most pronounced at 11 a.m. (33%) and 12 p.m. (20%). That is the biggest drawback of the proposed system. The positive thing is that the "drop downs" of A_{irr}-H around the equinox are significantly shallower at 10 a.m. (≥90%) and 1 p.m. (≥75%). Besides, in the period 10 a.m.-1 p.m. there is no need to move the reflector (y-H=1 m).

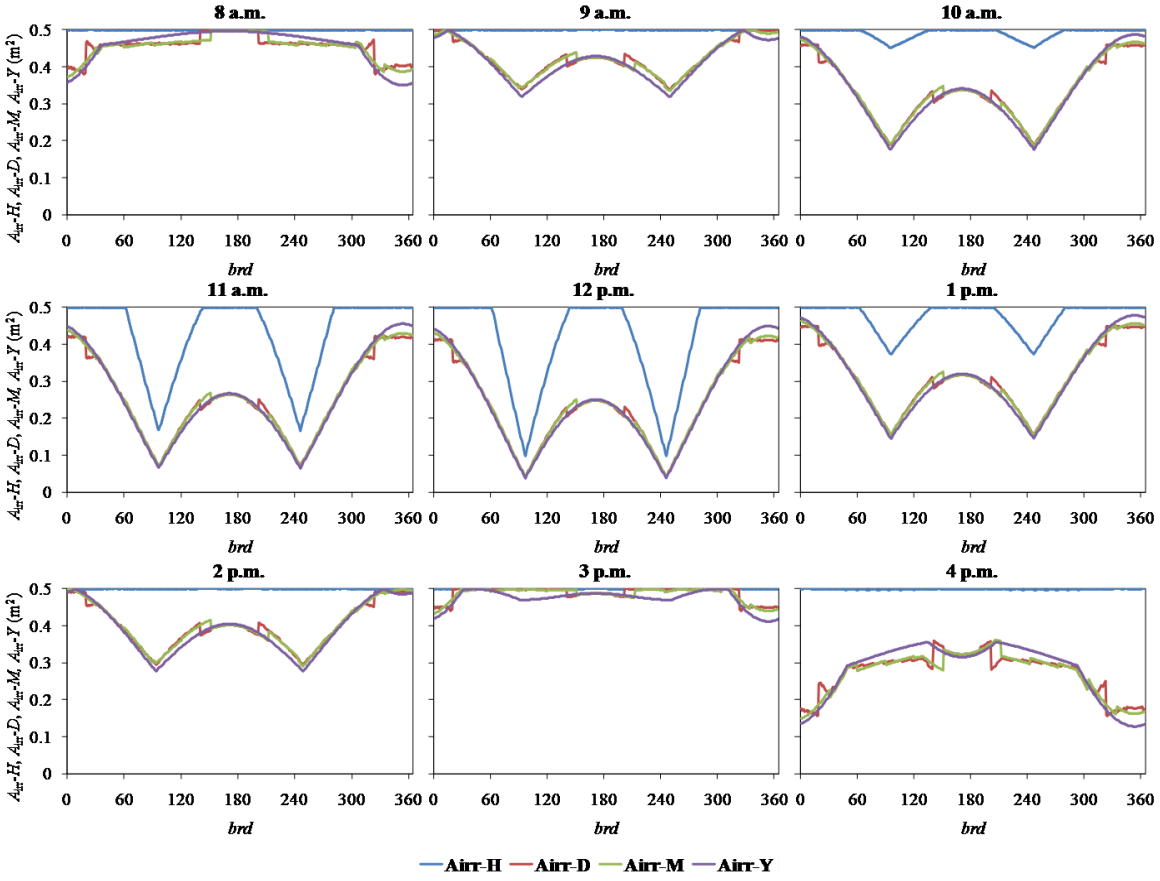

Figure 3. The values for the A_{irr} obtained according to the adopted y-H, y-D, y-M and y-Y

The main advantage of the second type of CRS is reflected in the fact that in the period around the summer and winter solstice, around noon, and in the morning and afternoon hours throughout the year, A_{irr}-H=0.5 m^2 (100%). Fig. 2 demonstrates that the differences between y-D, y-M and y-Y are very small. The explanation lies in the narrow range of y-D change, 0.34≤y-D≤0.44 m. The range of reflector movement on a monthly basis is 0.37≤y-M≤0.43 m, while the y-Y value is equal to 0.39 m. Due to the great similarities of the curves y-D, y-M and y-Y, the shape and values of the curves A_{irr}-D, A_{irr}-M and A_{irr}-Y (fig. 3) are approximately equal. It can be concluded that there is no reason why the reflector movement should be performed according to the optimal daily and monthly positions. The greatest advantage of such a CRS would be that the reflector would be fixed during the year. For 9 a.m.-2 p.m. and 4 p.m. on most days of the year, A_{irr}-D, A_{irr}-M and A_{irr}-Y have significantly lower values than A_{irr}-H. The smallest difference between them is in January and December (9 a.m.-2 p.m.) and at 8 and 3 p.m. throughout the year. The curves for 9 a.m.-2 p.m. have a similar shape, but in relation to those for 4 p.m. they differ, due to the position of the reflector, y-D, y-M and y-Y in relation to y-H. With the known A_{irr}-H, A_{irr}-D, A_{irr}-M and A_{irr}-Y, it is now possible to find the total solar radiation incident on the both a BSC (H'_{dG}) and a MSC (H'_{cG}) (fig. 4). In order to easily compare the

performance of the BSC and MSC, in fig. 5 the percentage difference between H'_{dG} and H'_{cG} ($\Delta H'$-H, $\Delta H'$-D, $\Delta H'$-M and $\Delta H'$-Y), expressed as $\Delta H' = 100 \cdot (H'_{dG} - H'_{cG}) / H'_{cG}$, are given.

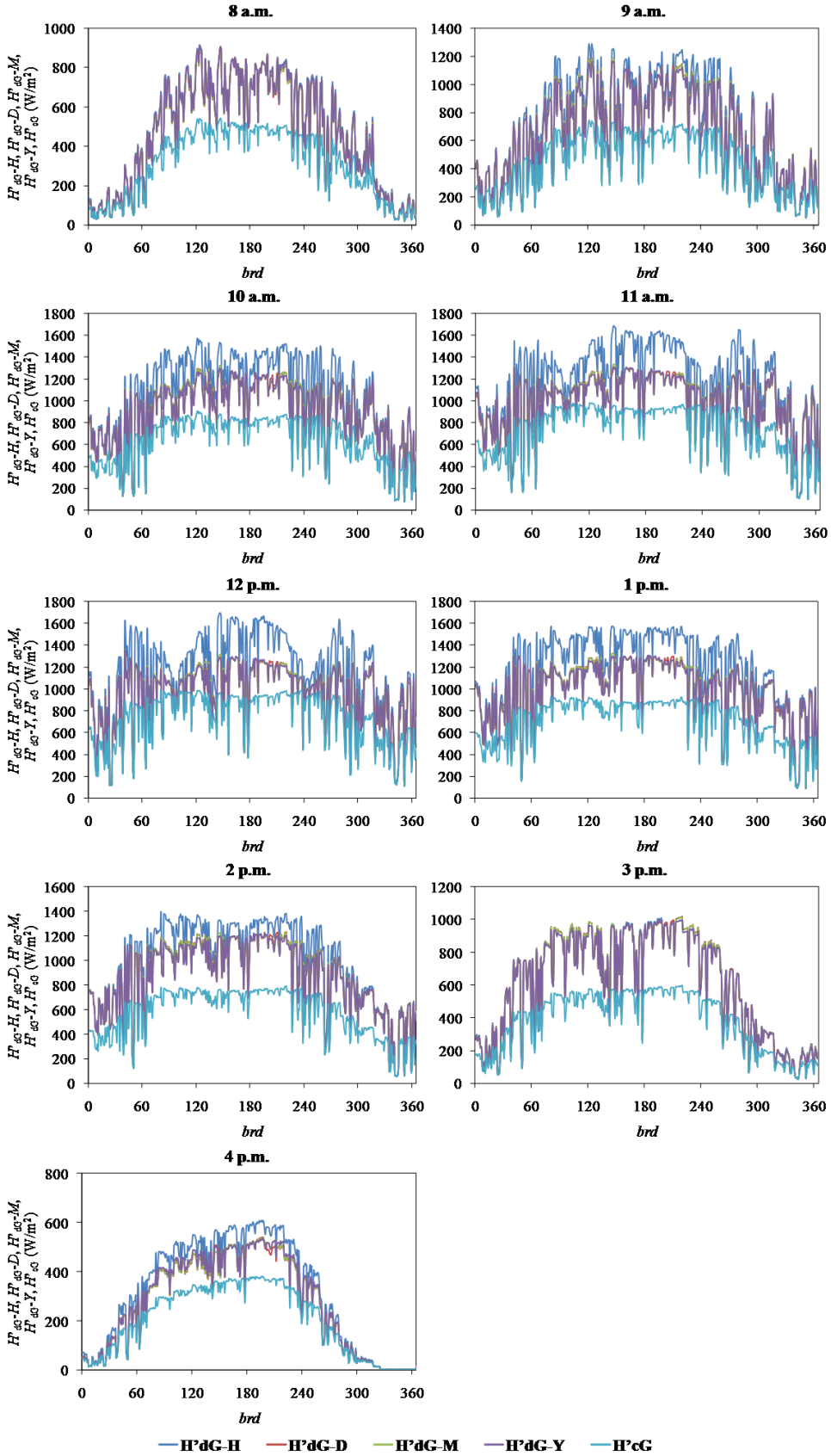

Figure 4. The values for the H'_{dG} (H'_{dG}-H, H'_{dG}-D, H'_{dG}-M, H'_{dG}-Y) and H'_{cG}

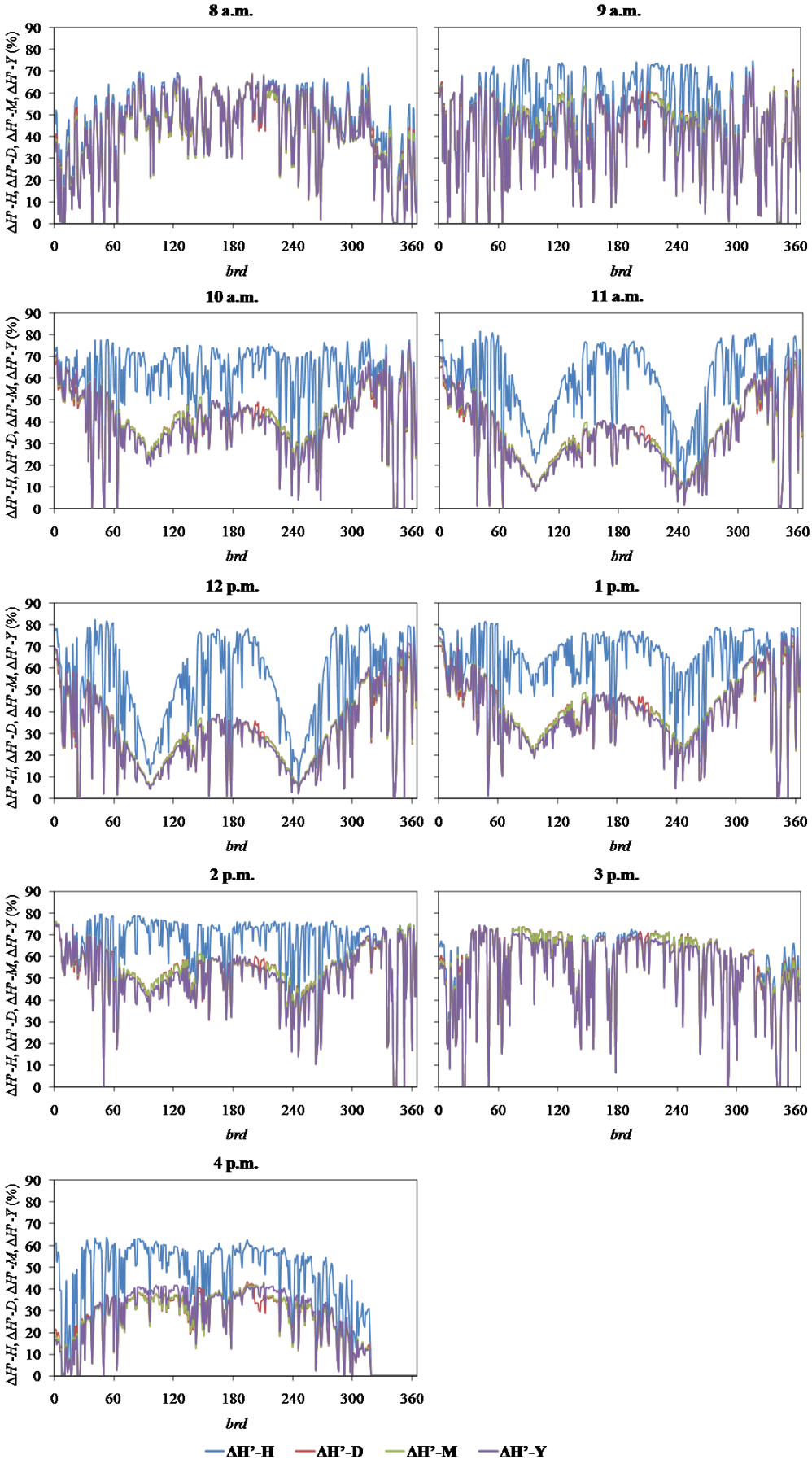

Figure 5. Percentage difference between H'_{dG} and H'_{cG}: Δ*H'-H*, Δ*H'-D*, Δ*H'-M* and Δ*H'-Y*

The diagrams shown in fig. 2-5 cannot be observed separately. The two variables that have the greatest influence on the shape and values of the curves for H'_{dG} and $\Delta H'$ are A_{irr} and share of diffuse radiation in the total incident solar radiation ($D=H'_{dif}/(H'_{dir}+H'_{dif})$). With the full irradiation of the BLAS and ρ=0.9, the theoretically largest percentage difference $\Delta H'$ would be 90%, but under the condition that H'_{dif}=0. However, in reality this is not the case ($H'_{dif}>0$). Hence, $\Delta H'\leq 90\%$ for all hours and days of the year. A smaller *D*, but at full irradiation of the BLAS, contributes to a higher performance of the BSC or a greater $\Delta H'$ and vice versa. Although the reflection of diffuse radiation is neglected, it is to be expected that a small part of it would be reflected on the BLAS, which would make the BSC performance to be a little better. For all hours and days of the year, the BSC exhibits a significantly better performance than the MSC, regardless of the way the reflector is moved either according to optimal hourly or annual positions. The curves for $\Delta H'$-*H*, $\Delta H'$-*D*, $\Delta H'$-*M* and $\Delta H'$-*Y* follow the curves for A_{irr}-*H*, A_{irr}-*D*, A_{irr}-*M* and A_{irr}-*Y*. It is observed that the values for H'_{dG} and $\Delta H'$ vary during the day and year even when A_{irr} is constant. This is a consequence of their dependence on the parameter *D*. In other words, the maximal peaks refer to the maximum possible A_{irr} and very low *D*. In hours with extremely high *D* the minimal peaks occur ($H'_{dG}\approx H'_{cG}$). The curves for $\Delta H'$-*D*, $\Delta H'$-*M* and $\Delta H'$-*Y* almost coincide, confirming once again that there is no need to move the reflector according to its optimal daily and monthly positions.

In order to accomplish the highest performance of the BSC it is recommended to move the reflector on hourly basis during the year. Comparing $\Delta H'$-*H* and $\Delta H'$-*Y*, the percentage increase for *y*-*H* is always greater than the increase for *y*-*Y*, under the condition of neglecting the moments when $H'_{dG}\approx H'_{cG}$. The highest achieved $\Delta H'$-*H* is in the range of 63.64-82.20%. On the most unfavorable dates for using this type of CRS (*brd*=97 and 246) at 11 a.m. and 12 p.m. the lowest $\Delta H'$-*H* values of 20% and 10% were recorded. However even then, $\Delta H'$-*H* was higher than $\Delta H'$-*Y* (9% (11 a.m.) and 5% (12 p.m.)). Although at 10 a.m. and 1 p.m. there are the "drop downs" of A_{irr}-*H*, they are milder and significantly less affected the amount of $\Delta H'$-*H*. Namely, for both hours and dates, $\Delta H'$-$H\geq 50\%$. Generally speaking, the average annual $\Delta H'$-*H* is in the range of 44.85-65.15%.

The greatest advantage of the CRS whose reflector would be placed in a position that corresponds to the optimal annual position, is attributed to the fact that it is fixed. As already described this results in significantly lower values for $\Delta H'$-*Y* compared to $\Delta H'$-*H*. In other words, the average annual $\Delta H'$-*Y* is in the range of 27.90-53.69%. There are periods, January and December (9 a.m.-2 p.m.) and at 8 a.m. and 3 p.m., when their differences are relatively small, due to small deviations of *y*-*Y* from *y*-*H*. It can be concluded that there is a third way of using this type of CRS. Namely, in December and January, the reflector would be fixed, while in the rest of the year it would move according to the optimal hourly positions. This way of using reflector would have a smaller contribution than the first, but significantly higher than the second. Another fact that does not support the fixed position of the reflector is the energy performance of the BSC in the early morning (6 and 7 a.m.) and late afternoon hours (5 and 6 p.m.), which were neglected in this study. In the mentioned periods of the day due to lower solar altitude angle, *y*-*H* will be smaller than those obtained at 8 a.m. and 4 p.m.. The reflector will be closer to the BSC. Conversely, *y*-*Y* will be significantly greater than *y*-*H*. The large distance of the fixed reflector prevents the reflection of solar beams on the BLAS, which is why H'_{dG}-$Y\approx H'_{cG}$. This is supported by the results obtained for *y*-*H*, *y*-*Y*, A_{irr}-*H*, A_{irr}-*Y*, $\Delta H'$-*H* and $\Delta H'$-*Y* at 4 p.m., when *y*-*Y* was greater than *y*-*H*. However, $\Delta H'$-*H* will undoubtedly have relatively high amounts during these periods. The results illustrated in fig. 5 on hourly basis, can be

observed in another way, on daily basis (fig. 6). Fig. 6 shows daily increase in the total solar radiation for *y-H* and *y-Y*, throughout the year.

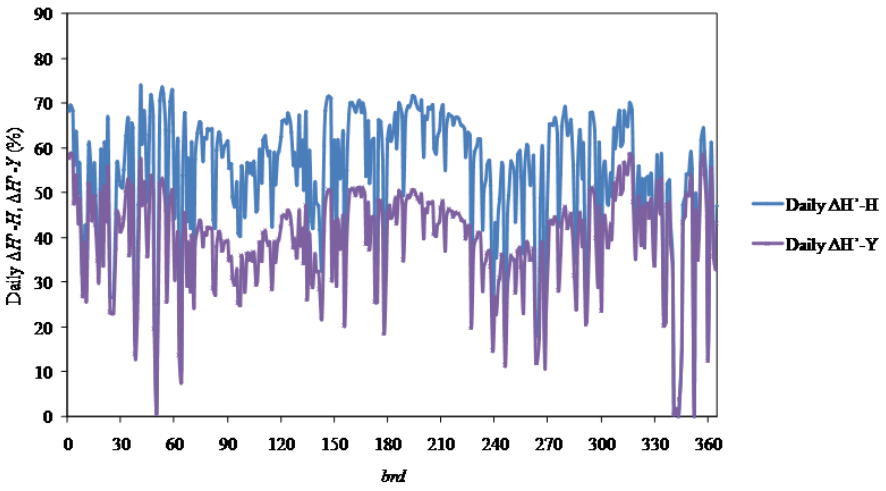

Figure 6. Daily percentage differences Δ*H*'-*H* and Δ*H*'-*Y*

The conclusions identical to those stated for fig. 5 can be drawn. In other words, A_{irr} and *D* have the greatest influence on the energy performance of the proposed CRS. There are four the "drop downs" of daily increases during the year. Those around the spring and autumn equinoxes are primarily the result of the effect of the parallelism between the collector and reflector (significantly lower A_{irr}), while the other two, in December and January, are caused by a large share of diffuse radiation (*D*). However, the daily increases for both *y-H* and *y-Y* are significant and reach a value of 74% and 59%, respectively. With known daily increases, it is possible to determine the monthly and annual increases. When it comes to the difference between monthly Δ*H*'-*H* and Δ*H*'-*Y*, the highest value was achieved in the month of July, on average around 19.7% (65.91% versus 46.21%). The smallest difference was recorded in December and January, of only 3.4% and 7.15%, respectively. For all other months, with the exception of November (8.1%) and February (13.8%), it averaged around 17.6%. Observed on an annual level, the energy performance of the considered BSC, either with an hourly movement of the reflector or with a fixed reflector, could be 54% and 39.4%, respectively, higher than that of a MSC. The findings of this research have shown the possitive effect of using single flat-plate reflector which is in parallel with the separated BSC. Considering the estimated hourly, daily, monthly and annual increase of the total solar radiation, it is believed that the proposed concept can outperform the similar concepts described in the research available in the scientific literature ([9,12,14-19,22,24,25]). The results from those studies and present work are compared and given in tab. 1.

Table 1. Comparison of the obtained findings with those from similar studies

Reference	BSC and reflector arrangement	Moveable/fixed reflector	Reflecting surface	Bifacial gain hourly (h); daily (d); annual (a)
[9]	tilted-separated	fixed	aluminum plate	48% (d) - 5 reflectors
[12]	tilted-separated	moveable	mirror	57% (d); 51% (a) - 2 reflectors
[14]	tilted-separated	fixed	aluminum foil	16.54% (d); 14.77% (a)
[15]	tilted-separated	fixed	aluminum foil	21.4% (d)
[16]	tilted-separated	fixed	white concrete	9.4% (a)
[17]	tilted-separated	moveable/fixed	mirror	30%/17% (a)
[18]	parallel-integrated	fixed	semimirror	20% (h)
[19]	parallel-integrated	fixed	mirror	26% (a)
[22]	parallel-separated	fixed	stainless steel	40% (d) - 3 reflectors
[24]	parallel-separated	fixed	mirror	10.85% (-)
[25]	parallel-separated	moveable	mirror	25.9% (h)
This study	parallel-separated	moveable/fixed	mirror	74%/59% (d); 54%/39.4% (a)

The bifacial gain is affected not only by the arrangement of the BSC and reflector, the position and material of the reflecting surface, but also by the size or number of the reflectors. The highest bifacial gain is achieved with the parallel-separated arangement, moveable and mirror reflecting surface. These are the characteristics of the proposed CRS. Satisfactory results are accomplished with tilted-separated arrangement but with multiple reflectors [9,12]. The main limitation of the previous studies relies on the fact that the optimization of the size and/or position of the reflector was not conducted. The parallel-integrated CRS design offers cost-effectiveness and simplicity of construction, but exhibits significantly lower bifacial performance. In terms of complexity, bulkiness and cost-effectiveness, the studied CRS can be in a more favorable position compared to the systems with considerable bifacial gain reported in [9,12,22]. Its construction would be smaller (A_r/A_c=4 versus A_r/A_c=7.6 [9] and A_r/A_c=6.7 [22]) and simpler because it has only one reflector. The CRS described in [12] consists of two separate manually moveable mirrors that occupy a larger area. Considering the data given in [23], the costs of the proposed CRS will be at least 39% higher than the costs of the corresponding MSC. Optimization of its production costs is the subject of future research.

4. Conclusions

This paper provides an analytical model for calculating the optimal size and hourly (*y-H*), daily (*y-D*), monthly (*y-M*) and annual positions (*y-Y*) of the flat-plate reflector placed in parallel below the bifacial solar collector (BSC) and moveable only in the direction normal to the collector plane. The daily, monthly and annual energy performance of the optimized bifacial collector-reflector system was estimated and compared with that of the corresponding monofacial solar collector (MSC). The main conclusions are summarized as follows:

- the optimal size of the reflector has to be four times larger than the collector size, in order for the irradiated area of the lower BSC surface (A_{irr}), at every moment (hour), would be the highest possible;
- the performance of the BSC at *y-Y* is almost identical to that at *y-D* and *y-M*, due to small differences between *y-D*, *y-M* and *y-Y* and the corresponding A_{irr}. In other words, two ways of use of the reflector are recommended, either according to the *y-H* (moveable reflector) or *y-Y* (fixed reflector);

- the A_{irr} and the share of diffuse radiation in the total solar radiation (D) are the two factors that most affect the BSC performance. The maximum A_{irr} and the minimum D ensure the highest performance of the BSC;
- with optimally positioned moveable or fixed reflector the total solar radiation incident on the BSC can be significantly higher than that for a MSC. Its largest daily and monthtly as well as average annual increase is: 74% (59%), 65.91% (46.21%) and 54% (39.4%), respectively;
- the proposed model can be applied to evaluate the energy performance of flat-plate bifacial thermal, PV or PVT solar collector, of arbitrary size and position, which is in this arrangement with a planar reflector.

Acknowledgements

This investigation is a part of the project TR 33015 of the Technological Development of the Republic of Serbia. We would like to thank the Ministry of Education, Science and Technological Development of the Republic of Serbia for their financial support during this investigation.

Appendix A. Mathematical model for determining the parameter A_{irr}

The form of the equations for A_{irr} depends on whether and how the reflected beams form the same area. Because of this dependence, terms such as full irradiation (FIRR) and partial irradiation (shading) (PIRR) are introduced:

$$A_{irr} = f(\mathrm{FIRR}, \mathrm{PIRR}) = \begin{cases} A_{irr} = \xi \cdot \lambda & \mathrm{FIRR}_{ewG\alpha} - \mathrm{FIRR}_{nsG\alpha} \\ A_{irr} = \xi \cdot a_p + \lambda \cdot b_{pnsG\alpha} & \mathrm{PIRR}_{ewG\alpha} - \mathrm{PIRR}_{nsG\alpha} \\ A_{irr} = \xi \cdot \lambda + \lambda \cdot b_{pnsG\alpha} & \mathrm{FIRR}_{ewG\alpha} - \mathrm{PIRR}_{nsG\alpha} \\ A_{irr} = \xi \cdot a_p & \mathrm{PIRR}_{ewG\alpha} - \mathrm{FIRR}_{nsG\alpha} \end{cases} \quad \text{(A1)}$$

The equations for $\beta_{nsG\alpha}$, $\beta_{ewG\alpha}$ and $\gamma_{G\alpha}$

First, the parameters $\beta_{nsG\alpha}$, $\beta_{ewG\alpha}$ and $\gamma_{G\alpha}$ should be found. Their calculation follows the calculation of the λ, ξ, a_p, $p_{nsG\alpha}$ ($p_{ewG\alpha}$) and $b_{pnsG\alpha}$:

$$\cos\beta_{nsG\alpha} = \frac{\cos G\cdot(-\cos\alpha\cdot\cos\beta\cdot\cos\gamma + \sin\alpha\cdot\cos\beta\cdot\sin\gamma) + \sin G\cdot\sin\beta}{\sqrt{[\cos G\cdot(-\cos\alpha\cdot\cos\beta\cdot\cos\gamma + \sin\alpha\cdot\cos\beta\cdot\sin\gamma) + \sin G\cdot\sin\beta]^2 + [\sin G\cdot(-\cos\alpha\cdot\cos\beta\cdot\cos\gamma + \sin\alpha\cdot\cos\beta\cdot\sin\gamma) - \cos G\cdot\sin\beta]^2}} \quad \text{(A2)}$$

$$\cos\beta_{ewG\alpha} = \frac{\cos\alpha\cdot\cos\beta\cdot\sin\gamma + \sin\alpha\cdot\cos\beta\cdot\cos\gamma}{\sqrt{[\cos\alpha\cdot\cos\beta\cdot\sin\gamma + \sin\alpha\cdot\cos\beta\cdot\cos\gamma]^2 + [\sin G\cdot(-\cos\alpha\cdot\cos\beta\cdot\cos\gamma + \sin\alpha\cdot\cos\beta\cdot\sin\gamma) - \cos G\cdot\sin\beta]^2}} \quad \text{(A3)}$$

$$\cos\gamma_{G\alpha} = \frac{\cos G\cdot(-\cos\alpha\cdot\cos\beta\cdot\cos\gamma + \sin\alpha\cdot\cos\beta\cdot\sin\gamma) + \sin G\cdot\sin\beta}{\sqrt{[\cos G\cdot(-\cos\alpha\cdot\cos\beta\cdot\cos\gamma + \sin\alpha\cdot\cos\beta\cdot\sin\gamma) + \sin G\cdot\sin\beta]^2 + [\cos\alpha\cdot\cos\beta\cdot\sin\gamma + \sin\alpha\cdot\cos\beta\cdot\cos\gamma]^2}} \quad \text{(A4)}$$

The well-known equations for the solar collector orientation (α), solar altitude (β) and solar azimuth angle (γ) are not presented.

The equations for λ (ξ)

For $L_r > L_c$, $L_r/2 < L_c$ and for $0^\circ < \gamma_{G\alpha} < 180^\circ$ (same as for $180^\circ < \gamma_{G\alpha} < 360^\circ$), $\mathrm{tg}(\beta^{*}_{ewG\alpha}) = y/(L_r/2 - L_c/2)$, $\mathrm{tg}(\beta^{**}_{ewG\alpha}) = y/(L_c/2)$ and $\mathrm{tg}(\beta^{***}_{ewG\alpha}) = y/(L_c/2 + L_r/2)$, it follows:

$$\text{PIRR}_{\text{ewG}\alpha}: 90° > \beta_{\text{ewG}\alpha} \geq \beta^{*}_{\text{ewG}\alpha} \Rightarrow \lambda = \frac{2y}{\text{tg}(\beta_{\text{ewG}\alpha})} \quad \text{(A5)}$$

$$\text{PIRR}_{\text{ewG}\alpha}: \beta^{*}_{\text{ewG}\alpha} > \beta_{\text{ewG}\alpha} > \beta^{**}_{\text{ewG}\alpha} \Rightarrow \lambda = \frac{y}{\text{tg}(\beta_{\text{ewG}\alpha})} + \frac{L_r - L_c}{2} \quad \text{(A6)}$$

$$\text{FIRR}_{\text{ewG}\alpha}: \beta^{**}_{\text{ewG}\alpha} \geq \beta_{\text{ewG}\alpha} > \beta^{***}_{\text{ewG}\alpha} \Rightarrow \lambda = \frac{L_c + L_r}{2} - \frac{y}{\text{tg}(\beta_{\text{ewG}\alpha})} \quad \text{(A7)}$$

For $\boldsymbol{L_r > L_c}$, $\boldsymbol{L_r/2 = L_c}$ and for $0^\circ < \gamma_{G\alpha} < 180^\circ$ (same as for $180^\circ < \gamma_{G\alpha} < 360^\circ$), $\text{tg}(\beta^{*}_{\text{ewG}\alpha}) = y/(L_c/2)$ and $\text{tg}(\beta^{**}_{\text{ewG}\alpha}) = y/(L_r/2 + L_c/2)$, it follows:

$$\text{PIRR}_{\text{ewG}\alpha}: 90° > \beta_{\text{ewG}\alpha} > \beta^{*}_{\text{ewG}\alpha} \Rightarrow \lambda = \frac{2y}{\text{tg}(\beta_{\text{ewG}\alpha})} \quad \text{(A8)}$$

$$\text{FIRR}_{\text{ewG}\alpha}: \beta^{*}_{\text{ewG}\alpha} \geq \beta_{\text{ewG}\alpha} > \beta^{**}_{\text{ewG}\alpha} \Rightarrow \lambda = \frac{L_c + L_r}{2} - \frac{y}{\text{tg}(\beta_{\text{ewG}\alpha})} \quad \text{(A9)}$$

For $\boldsymbol{L_r > L_c}$, $\boldsymbol{L_r/2 > L_c}$ and for $0^\circ < \gamma_{G\alpha} < 180^\circ$ (same as for $180^\circ < \gamma_{G\alpha} < 360^\circ$), $\text{tg}(\beta^{*}_{\text{ewG}\alpha}) = y/(L_c/2)$, $\text{tg}(\beta^{**}_{\text{ewG}\alpha}) = y/(L_r/2 - L_c/2)$ and $\text{tg}(\beta^{***}_{\text{ewG}\alpha}) = y/(L_r/2 + L_c/2)$, it follows:

$$\text{PIRR}_{\text{ewG}\alpha}: 90° > \beta_{\text{ewG}\alpha} > \beta^{*}_{\text{ewG}\alpha} \Rightarrow \lambda = \frac{2y}{\text{tg}(\beta_{\text{ewG}\alpha})} \quad \text{(A10)}$$

$$\text{FIRR}_{\text{ewG}\alpha}: \beta^{*}_{\text{ewG}\alpha} \geq \beta_{\text{ewG}\alpha} \geq \beta^{**}_{\text{ewG}\alpha} \Rightarrow \lambda = L_c \quad \text{(A11)}$$

$$\text{FIRR}_{\text{ewG}\alpha}: \beta^{**}_{\text{ewG}\alpha} > \beta_{\text{ewG}\alpha} > \beta^{***}_{\text{ewG}\alpha} \Rightarrow \lambda = \frac{L_c + L_r}{2} - \frac{y}{\text{tg}(\beta_{\text{ewG}\alpha})} \quad \text{(A12)}$$

The equations for λ for the interval $0^\circ < \gamma_{G\alpha} < 180^\circ$ ($180^\circ < \gamma_{G\alpha} < 360^\circ$) correspond to the equations for ξ but for the interval $90^\circ < \gamma_{G\alpha} < 270^\circ$ ($270^\circ < \gamma_{G\alpha} < 90^\circ$). Also, the parameters L_c, L_r and $\beta_{\text{ewG}\alpha}$ should be replaced by the parameters W_c, W_r and $\beta_{\text{nsG}\alpha}$. These equations cannot be used for the limit values of the $\gamma_{G\alpha} = 0^\circ, 90^\circ, 180^\circ, 270^\circ, 360^\circ$, for which $\beta_{\text{ewG}\alpha} = 90^\circ$ ($\gamma_{G\alpha} = 0^\circ, 180^\circ$ or 360°) and $\beta_{\text{nsG}\alpha} = 90^\circ$ ($\gamma_{G\alpha} = 90^\circ$ or 270°). Then the irradiated area is calculated as $A_{\text{irr}} = \xi \cdot \lambda_0$ and $A_{\text{irr}} = \xi_0 \cdot \lambda$, where $\lambda_0 = L_c$ and $\xi_0 = W_c$.

The equations for $\boldsymbol{p_{\text{nsG}\alpha}}$ ($\boldsymbol{p_{\text{ewG}\alpha}}$), $\boldsymbol{a_p}$ and $\boldsymbol{b_{\text{pnsG}\alpha}}$

The parameter $p_{\text{nsG}\alpha}$ ($p_{\text{ewG}\alpha}$) appears only for the PIRR situation: $p_{\text{nsG}\alpha} = y/\text{tg}\beta_{\text{nsG}\alpha}$ and $p_{\text{ewG}\alpha} = y/\text{tg}\beta_{\text{ewG}\alpha}$. The equations of the a_p, for the situations $\text{PIRR}_{\text{ewG}\alpha}$-$\text{PIRR}_{\text{nsG}\alpha}$, and for the interval $0^\circ < \gamma_{G\alpha} < 90^\circ$ are presented below. For the intervals, $90^\circ < \gamma_{G\alpha} < 180^\circ$, $180^\circ < \gamma_{G\alpha} < 270^\circ$ and $270^\circ < \gamma_{G\alpha} < 360^\circ$, the equations are identical with the difference that the angle $\gamma_{G\alpha}$ is replaced by the angles $180^\circ - \gamma_{G\alpha}$, $\gamma_{G\alpha} - 180^\circ$ and $360^\circ - \gamma_{G\alpha}$, respectively:

For $0^\circ < \gamma_{G\alpha} < 90^\circ$, $\text{tg}(\gamma_{G\alpha})^{*} = 0$ and $\text{tg}(\gamma_{G\alpha})^{**} = ((L_r - L_c)/2)/p_{\text{nsG}\alpha}$ it follows

$$\text{tg}(\gamma_{G\alpha})^{*} \leq \text{tg}(\gamma_{G\alpha}) \leq \text{tg}(\gamma_{G\alpha})^{**} \Rightarrow a_p = L_c \quad \text{(A13)}$$

$$\text{tg}(\gamma_{G\alpha}) > \text{tg}(\gamma_{G\alpha})^{**} \Rightarrow a_p = \frac{L_c + L_r}{2} - \text{tg}(\gamma_{G\alpha}) \cdot p_{\text{nsG}\alpha} \quad \text{(A14)}$$

For the combination of the situations $PIRR_{ewG\alpha}$-$FIRR_{nsG\alpha}$, a_p is calculated as $a_p=L_c-2\cdot p_{ewG\alpha}+\lambda$. As for the parameter $b_{pnsG\alpha}$ there is only one equation, $b_{pnsG\alpha}=W_c-2\cdot p_{nsG\alpha}$.

Nomenclature

A - area [m^2]
a_p - length of irradiation in the CRS plane [m]
b_p - length of shadow [m]
brd - day of the year [-]
G - collector tilt angle [rad]
H' - intensity of the hourly solar radiation on a horizontal surface [W/m^2]
H'_G - intensity of the hourly solar radiation on a tilted surface [W/m^2]
i - incident angle of the solar beam [rad]
L - length [m]
p - length parameter [m]
W - width [m]
y - distance between the collector and reflector planes [m]
Greek symbols
α - collector orientation [rad]
β - solar altitude angle [rad]
$\beta_{ewG\alpha}$ - projection of the solar altitude angle on the EWGα plane [rad]
$\beta_{nsG\alpha}$ - projection of the solar altitude angle on the NSGα plane [rad]
γ - solar azimuth angle [rad]
$\gamma_{G\alpha}$ - projection of the solar azimuth angle on the CRS plane [rad]
$\Delta H'$ - percentage difference between the total solar radiation incident on a bifacial solar collector and that incident on a monofacial solar collector [%]
λ - length of irradiation in the EWGα plane [m]
ξ - length of irradiation in the NSGα plane [m]
ρ - coefficient of reflection [-]
Subscripts
c - monofacial (conventional) solar collector
d - bifacial solar collector
dif - diffuse solar radiation
dir - direct solar radiation
ewGα - in the EWGα plane
irr - irradiated
low - lower
nsGα - in the NSGα plane
r - reflector
up - upper
Abbreviations
BFPC - bifacial flat-plate solar thermal collector
BLAS - lower surface of the bifacial solar collector
BPV - bifacial photovoltaic

BPVT - bifacial photovoltaic thermal
BSC - bifacial solar collector
CRS - collector-reflector system
FPC - flat-plate solar thermal collector
MSC - monofacial (conventional) solar collector
PV - photovoltaic
PVT - photovoltaic thermal

References

[1] Ahmad, A., *et al*., Parabolic trough solar collectors: A sustainable and efficient energy source, *Mater Sci Energy Technol, 7* (2024), pp. 99-106, DOI: 10.1016/j.mset.2023.08.002

[2] Qiu, G., *et al*., Comparative study on solar flat-plate collectors coupled with three types of reflectors not requiring solar tracking for space heating, *Renew Energy, 169* (2021), pp. 104-116, DOI: 10.1016/j.renene.2020.12.134

[3] Agrawal, M., *et al*., Performance analysis of photovoltaic module with reflector: Optimizing orientation with different tilt scenarios, *Renew Energy, 186* (2022), pp. 10-25, DOI: 10.1016/j.renene.2021.12.149

[4] El‐Assal, B., *et al*., Effect of Side Reflectors on the Performance of Flat Plate Solar Collector: A Case Study for Asir Region, Saudi Arabia, *Arab J Sci Eng, 45* (2020), pp. 1035-1050, DOI: 10.1007/s13369-019-04221-x

[5] Khan, M.A., *et al*., Performance Evaluation of Photovoltaic Solar System with Different Cooling Methods and a Bi-Reflector PV System (BRPVS): An Experimental Study and Comparative Analysis, *Energies, 10(6):826* (2017), DOI: 10.3390/en10060826

[6] Ahmed, O.K., Bawa, S.M., Reflective mirrors effect on the performance of the hybrid PV/thermal water collector, *Energy for Sustainable Development, 43* (2018), pp. 235-246, DOI: 10.1016/j.esd.2018.02.001

[7] Pavlović, Z.T., Kostić, L.T., Variation of reflected radiation from all reflectors of a flat plate solar collector during a year, *Energy, 80* (2015), pp. 75-84, DOI: 10.1016/j.energy.2014.11.044

[8] Rachedi, M.Y., *et al*., A novel model for optimizing tilts of four reflectors on a flat plate thermal collector: Case study in Ouargla region, *Case Stud Therm Eng, 32:101872* (2022), DOI: 10.1016/j.csite.2022.101872

[9] Souka, A.F., Double exposure flat-plate collector, *Sol Energy, 9* (1965), 3, pp. 117-118, DOI: 10.1016/0038-092X(65)90083-6

[10] Souka, A.F., Safwat, H.H., Theoretical evaluation of the performance of a double exposure flat-plate collector using a single reflector, *Sol Energy, 12* (1969), 3, pp. 347-352, DOI: 10.1016/0038-092X(69)90048-6

[11] Durković, V., Đurišić, Ž., Impact of a horizontal reflector on the techno-economic characteristics of large VPV power plants, *Sol Energy, 220* (2021), pp. 650-659, DOI: 10.1016/j.solener.2021.03.069

[12] Zahid, M.A., *et al*., A novel approach for power enhancement of vertical mounted bifacial photovoltaic system using reflecting mirrors, *J Clean Prod, 397:136541* (2023), DOI: 10.1016/j.jclepro.2023.136541

[13] Khan, M.R., *et al*., Vertical bifacial solar farms: Physics, design, and global optimization, *Appl Energy, 206* (2017), pp. 240-248, DOI: 10.1016/j.apenergy.2017.08.042

[14] Gu, W., *et al*., Experimental investigation of the bifacial photovoltaic module under real conditions, *Renew Energy, 173* (2021), pp. 1111-1122, DOI: 10.1016/j.renene.2020.12.024

[15] Ganesan, K., *et al*., Performance analysis of n-type PERT bifacial solar PV module under diverse albedo conditions, *Sol Energy, 252* (2023), pp. 81-90, DOI: 10.1016/j.solener.2023.01.020

[16] Chen, H., *et al*., Experimental and simulation study on bifacial photovoltaic modules integration with buildings, *Therm Sci, 26* (2022), 5B, pp. 4413-4422, DOI: 10.2298/TSCI220122088C

[17] Wang, S., *et al*., Efficiency Enhancement of Tilted Bifacial Photovoltaic Modules with Horizontal Single-Axis Tracker - The Bifacial Companion Method, *Energies, 15(4):1262* (2022), DOI: 10.3390/en15041262

[18] Ooshaksaraei. P., *et al*., Characterization of a Bifacial Photovoltaic Panel Integrated with External Diffuse and Semimirror Type Reflectors, *International J Photoenergy, 2013:465837* (2013), DOI: 10.1155/2013/465837

[19] Lo, C.K., *et al*., New integrated simulation tool for the optimum design of bifacial solar panel with reflectors on a specific site, *Renew Energy, 81* (2015), pp. 293-307, DOI: 10.1016/j.renene.2015.03.047

[20] Mustapha, M., *et al*., Mathematical Modelling of Bifacial Photovoltaic-Thermal (BPVT) Collector with Mirror Reflector, *International J Renew Energy Res, 10* (2020), 2, DOI: 10.20508/ijrer.v10i2.10603.g7936

[21] Ooshaksaraei, P., *et al*., Performance of four air-based photovoltaic thermal collectors configurations with bifacial solar cells, *Renew Energy, 102* (2017), pp. 279-293, DOI: 10.1016/j.renene.2016.10.043

[22] Robles-Ocampo, B., *et al*., Photovoltaic/thermal solar hybrid system with bifacial PV module and transparent plane collector, *Sol Energy Mater Sol Cells, 91* (2007), 20, pp. 1966-1971, DOI: 10.1016/j.solmat.2007.08.005

[23] Nikolić, N., Lukić, N., Theoretical and experimental investigation of the thermal performance of a double exposure flat-plate solar collector, *Sol Energy, 119* (2015), pp. 100-113, DOI: 10.1016/j.solener.2015.06.038

[24] Saha, S.N., Sharma, S.P., Performance analysis of double-flow double-exposure solar air heater, *J Mech Sci Technol, 32* (2018), 3, pp. 1407-1414, DOI: 10.1007/s12206-018-0244-3

[25] Mandal, S., Ghosh, S.K., Experimental investigation of the performance of a double pass solar water heater with reflector, *Renew Energy, 149* (2020), pp. 631-640, DOI: 10.1016/j.renene.2019.11.160

[26] Nikolić, N., Lukić, N., A mathematical model for determining the optimal reflector position of a double exposure flat-plate solar collector, *Renew Energy*, *51* (2013), pp. 292-301, DOI: 10.1016/j.renene.2012.09.034

[27] Skerlić, J., Bojić, M., Optimization of solar collector performance by using EnergyPlus and Hooke-Jeeves algorithm, *Proceedings*, 41st International Congress on Heating, Refrigerating and Air-conditioning, Belgrade, Serbia, 2010, pp. 472-479

[28] ***, Climate data, https://climate.onebuilding.org/

RECEIVED DATE: 23.1.2024.
DATE OF CORRECTED PAPER: 23.02.2024
DATE OF ACCEPTED PAPER: 09.3.2024